

Real-Time Quality Assessment of Pediatric MRI via Semi-Supervised Deep Nonlocal Residual Neural Networks

Siyuan Liu, *Member, IEEE*, Kim-Han Thung, Weili Lin, Pew-Thian Yap, *Senior Member, IEEE*, Dinggang Shen, *Fellow, IEEE*

Abstract—In this paper, we introduce an image quality assessment (IQA) method for pediatric T1- and T2-weighted MR images. IQA is first performed slice-wise using a nonlocal residual neural network (NR-Net) and then volume-wise by agglomerating the slice QA results using random forest. Our method requires only a small amount of quality-annotated images for training and is designed to be robust to annotation noise that might occur due to rater errors and the inevitable mix of good and bad slices in an image volume. Using a small set of quality-assessed images, we pre-train NR-Net to annotate each image slice with an initial quality rating (i.e., pass, questionable, fail), which we then refine by semi-supervised learning and iterative self-training. Experimental results demonstrate that our method, trained using only samples of modest size, exhibit great generalizability, capable of real-time (milliseconds per volume) large-scale IQA with near-perfect accuracy.

Index Terms—Image quality assessment, nonlocal residual networks, semi-supervised learning, self-training

I. INTRODUCTION

Structural magnetic resonance imaging (sMRI) is widely used for brain morphological analysis due to its high spatial-resolution details of anatomical structures. However, sMRI is susceptible to image artifacts caused for instance by eye and head motion, hemodynamic changes, and magnetic field inhomogeneities [1]. Among these artifacts, motion artifacts are particularly prevalent when scanning pediatric subjects. As poor-quality images may bias subsequent analysis and result in incorrect conclusions, it is vital to correctly identify problematic images and exclude them from analysis.

Image quality assessment (IQA) is an important step to determine whether the acquired data are usable and whether a re-scan is necessary. IQA can be performed subjectively by a human rater or objectively by a computer algorithm. The most commonly used subjective quality ratings can be grouped into two categories, i.e., 1) score-based rating, where a visual quality score metric, such as Mean Opinion Score (MOS) [2], is used for quality grading; and 2) class-based rating, where a visual quality class spectrum, such as Excellent/Very Good/Good/Fair/Poor/Unusable [3] or Pass (Excellent to Very Good)/Questionable (Good to Fair)/Fail (Poor to Unusable) [4], is used for quality grading. Subjective IQA with visual

S. Liu, K.-H. Thung, W. Lin, P.-T. Yap and D. Shen are with the Department of Radiology and Biomedical Research Imaging Center (BRIC), University of North Carolina at Chapel Hill, NC, U.S.A. D. Shen is also with the Department of Brain and Cognitive Engineering, Korea University, Seoul, Korea.

Corresponding authors: ptyap@med.unc.edu, dgshen@med.unc.edu

inspection, even when carried out by experienced radiologists, is time-consuming, labor-intensive, costly, and error-prone [5]. Therefore, a reliable, accurate, and fully-automated objective IQA of sMRI is highly desirable.

Based on the availability of a reference image, objective IQA can be grouped into three categories, i.e., (i) full-reference IQA (FR-IQA), which requires a pristine image as reference; (ii) reduced-reference IQA (RR-IQA), which requires partial information from a reference image; and (iii) no-reference IQA (NR-IQA) or blind IQA, which requires no reference image. FR-IQA measures the quality of an image by comparing it with a reference using some evaluation metrics. On the other hand, RR-IQA uses only a limited number of features extracted from a reference [6] to provide a near FR-IQA performance. However, FR-IQA and RR-IQA have limited practical application as full or partial information from a pristine reference image is not always available. For quality assessment without any reference image, as in our case, NR-IQA [7] is needed. Currently, most NR-IQA methods [8–10] are designed for natural 2D images. MR images are typically 3D with intensity distributions and artifacts that are very different from natural images.

Recently, deep neural networks (DNNs), particularly convolutional neural networks (CNNs), have demonstrated great potential for IQA [11]. Instead of hand-crafted features, CNNs automatically learn image features that are pertinent to IQA. However, the performance of these deep learning methods generally depends on a large number of correctly labeled training samples, which are typically lacking for medical images, as labeling involves a huge amount of effort from experts. For example, it is labor-intensive and time-consuming to annotate quality scores for all the image slices in MR images to train a slice-wise IQA network. Thus, annotation is typically performed volume-wise, where each MR volume is associated with a single quality label. This is however inaccurate since each volume might contain a mix of good or bad slices.

In this paper, we address the above issues by introducing a deep learning based slice- and volume-wise IQA method that is robust to annotation errors and requires only a small amount of annotated images for training. To the best of our knowledge, this is the first work on deep learning based slice- and volume-wise NR-IQA of sMRI with explicit consideration of limited training samples and labeling noise. The key features of our method are summarized as follows:

- 1) Our method consists of a nonlocal residual neural net-

work (NR-Net) for slice-wise IQA and a random forest to agglomerate the slice IQA results for volume-wise IQA. We train our NR-Net using the slices of annotated image volumes, effectively increasing training sample size.

- 2) We employ depthwise separable residual (DSRes) blocks [12] and nonlocal residual (NRes) blocks [13] to construct the NR-Net. Compared to residual networks with standard convolutions, the computation-reduction property of the DSRes block and also the information fusion property of the NRes block make NR-Net much lighter, hence allowing fast real-time IQA.
- 3) We utilize semi-supervised learning to deal with the scenario where we have a small amount of labeled data but a large amount of unlabeled data. With a small number of labeled samples, we pre-train the NR-Net to label the slices of unlabeled volumes, which are then used to re-train the NR-Net.
- 4) We use an iterative self-training mechanism to prune or relabel unreliable labels to improve training effectiveness. Self-training is iterated until convergence.

The rest of this paper is organized as follows. In Section II, we briefly review related work on NR-IQA. Section III describes the NR-Net architecture, semi-supervised learning, and slice/volume self-training. We present the experimental results in Section IV and conclude this paper in Section V.

II. RELATED WORK

A. Deep Learning NR-IQA

Deep learning NR-IQA methods can be either score-based or class-based [14]. Score-based methods predict continuous-valued quality ratings, typically by treating quality assessment as a regression problem. Deep learning NR-IQA methods in this category (mostly for 2D natural images) [15–19] are typically trained image-wise and thus a large number of annotated images are needed. Patch-wise methods [20–23] use image patches as training samples, thus effectively increasing sample size.

Class-based methods [24–33] predict discrete-valued quality categories, often associated with human perception on image quality. Quality annotation in structural MRI is carried out manually via visual inspection. There is no reliable metric that can be used to provide continuous-valued quality ratings. Therefore, our IQA method is based on classification instead of regression to predict quality categories of slices and volumes.

B. Label Noise

Expert annotations are not always accurate, thus leading to “label noise”. Methods to cope with label noise can be divided into three categories [34]: 1) designing a robust loss, 2) cleansing noisy data, and 3) modeling the label noise distribution.

First, loss function can be reweighted or rectified to be robust to label noise [35–37].

Second, label noise can be “cleaned” before training, by either relabeling or removing mislabeled data [38, 39]. Removing mislabeled data, while shown to be effective [38, 39],

reduces sample size and hence degrade training effectiveness. Data cleansing is also affected by data imbalance [40], where minority classes may more likely be entirely removed. In comparison, relabeling mislabeled data maintains the sample size, but incorrect relabeling may lead to performance degradation.

Third, if some information about the label noise is available, it is possible to predict the distribution of label noise and use it to improve the classifier. Explicitly modeling or learning the label noise distribution [41–44] allows noisy labels to be detected and discarded during training. However, this approach depends on the accuracy of the label noise model, increases the complexity of learning algorithms, and may result in overfitting due to additional model parameters.

III. ARCHITECTURE

Fig. 1 shows an overview of our sMRI IQA method, which consists of two stages, i.e., slice assessment stage and volume assessment stage. The slice assessment stage is designed to predict the quality rating of each slice and is trained using semi-supervised learning and slice self-training. The volume assessment stage, trained using volume self-training, evaluates the quality rating of each volume by ensembling the quality ratings of slices belonging to this volume. Details of our method are described next.

A. Slice Quality Assessment Network

Our slice quality assessment network is designed with both accuracy and speed in mind. Fig. 2 shows the proposed network, NR-Net, which consists of four types of network blocks, i.e., convolution (Conv), depthwise separable residual (DSRes), nonlocal residual (NRes), and classifier blocks. The Conv and DSRes blocks extract low- and high-level features, respectively, whereas the NRes block [13] computes the response function at each position as a weighted summation of features from different spatial locations. The classifier block (realized with a convolutional layer, global average pooling, and a softmax activation function) outputs three probability values indicating whether a slice is “pass”, “questionable”, or “fail”. The slice is finally annotated with the label associated with the highest probability.

1) *DSRes Block*: We construct the DSRes block by integrating depthwise separable convolution (DSConv) layers in the NR-Net (blue in Fig. 2). Fig. 3(a) shows how a standard convolution layer filters all input channels and combine the results in an output channel. In comparison, a DSConv layer filters using a combination of depthwise convolution and pointwise convolution. Specifically, depthwise convolution performs channel-wise spatial convolution and concatenation, as shown in Fig. 3(b). Pointwise convolution subsequently projects the channels by depthwise 1×1 convolution onto a new channel, as shown in Fig. 3(c).

Based on Fig. 3, we show that DSConv is computationally more efficient than standard convolution. Given a c -channel $h \times w$ input feature map, a c' -channel $h' \times w'$ output feature map, and a $d \times d$ kernel, the computational cost (CC) of a standard convolution layer is given by $CC_{StdConv} = cc'd^2h'w'$. In contrast, the computational cost of a DSConv layer with

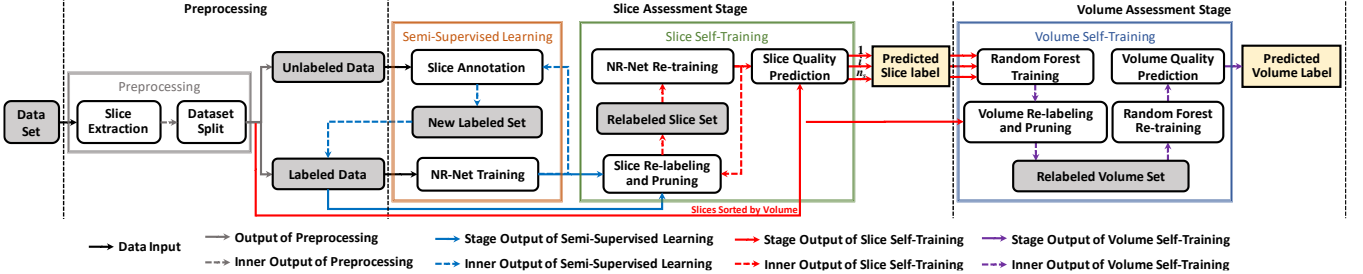


Fig. 1. Overview of our sMRI IQA method.

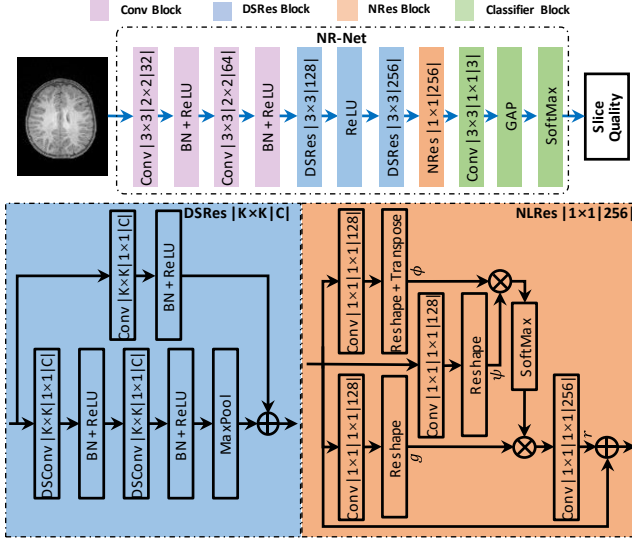


Fig. 2. Architecture of NR-Net, which consists of four types network blocks, i.e., the convolution (Conv), depthwise separable residual (DSRes), nonlocal residual (NRes), and classifier blocks. The parameters of DSRes and NRes blocks are denoted in the following format: “DSRes/NRes | kernel size | output channel |”, and the parameters of the convolution and depthwise separable convolution layers are similarly denoted as “Conv/DSConv | kernel size | strides | output channel |”. \otimes : matrix multiplication, \oplus : element-wise summation.

the same input and output, as shown in Fig. 3(b) and (c), is given by $CC_{DSConv} = cd^2 h'w' + cc'h'w'$. The computational reduction factor (CRF) of replacing standard convolution with DSConv is therefore given as $CRF_{conv} = 1/c' + 1/d^2$. Furthermore, the CRF of replacing a residual block constructed by standard convolutions with a DSRes block is $CRF_{DSRes} \approx 1/c' + 3/(2d^2 + 1)$ with $c' = 2c$. We use a 3×3 convolution kernel ($d = 3$) in each DSRes block, so that the computational cost of a DSRes block is 6 to 7 times smaller than that of a residual block with standard convolution.

2) *NRes Block*: The quality of an image slice is determined by the existence of artifacts at different spatial locations. We employ a nonlocal residual (NRes) block [13] in our network (orange in Fig. 2) to capture information from potentially distant locations. Given a c -channel $h \times w$ input feature map x , the output at the i -th location, $r_i \in \mathbb{R}^c$, of the NRes block is computed as the weighted sum of all features:

$$r_i = \frac{1}{C(x_i)} \sum_{\forall j} f(x_i, x_j)g(x_j), \quad x_i, x_j \in \mathbb{R}^c \quad (1)$$

where the weight function $f(\cdot, \cdot)$ encodes the pairwise similarity between feature vectors at locations i and j , $g(\cdot)$ computes a representation of a feature vector, and $C(x_i) = \sum_{\forall j} f(x_i, x_j)$ is a normalization factor. In this work, the weight function $f(x_i, x_j)$ is defined as

$$f(x_i, x_j) = \exp [\phi^T(x_i)\psi(x_j)], \quad (2)$$

where $\phi(\cdot)$ and $\psi(\cdot)$ are unary kernel functions that are implemented with 1×1 convolution kernels, thus making $\frac{1}{C(x_i)} f(x_i, x_j)$ a softmax function. The NRes block is incorporated in the NR-Net using a residual form.

NR-Net is lighter with less parameters by employing DSRes blocks and captures long-range dependencies between features regardless of their positional distances. Batch normalization and global average pooling are used for regularization without dropout to speed up training.

B. Semi-Supervised Learning

We employ semi-supervised learning to make full use of a small amount of labeled data and a large amount of unlabeled data. This is done by progressive annotation of unlabeled slices to retrain the network (orange box in Fig. 1). We begin by utilizing the NR-Net pre-trained with the labeled dataset to predict the “pass”, “questionable”, or “fail” probabilities of the slices of the unlabeled volumes. Each slice is annotated with the quality rating associated with the maximal probability. The labeled slices are then merged into the original labeled dataset to be used for retraining of the NR-Net.

C. Slice Self-Training

To deal with noisy labels, we propose a slice self-training method to sample “clean” data for training. This involves iterative slice relabeling/pruning and NR-Net retraining (green box in Fig. 1). Slices are quality-predicted using the pre-trained NR-Net and then selected based on the following conditions: 1) Predicted labels that are identical to those predicted in the previous iteration; 2) Predicted labels with high-confidence, i.e., maximal probabilities beyond a threshold. The labels of the selected slices are replaced with the predicted labels. Slices that do not meet these criteria are pruned from the training dataset. NR-Net is then retrained for the next iteration until accuracy improvement is minimal.

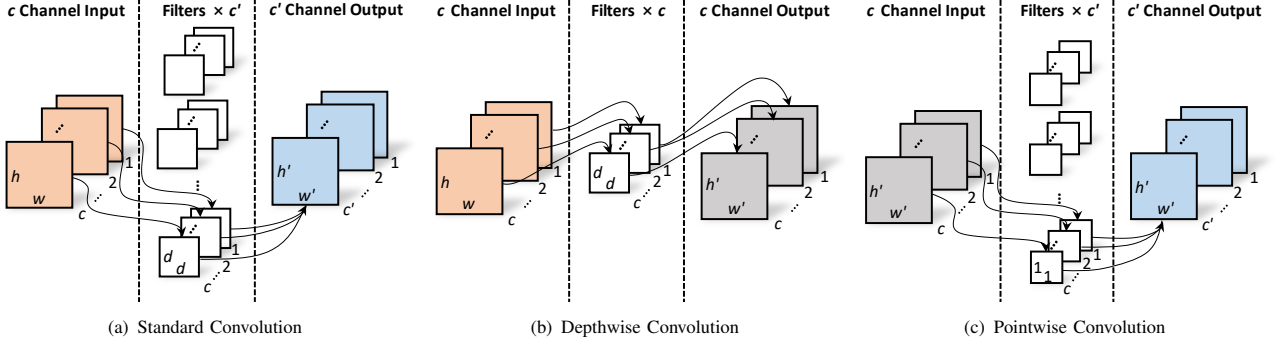


Fig. 3. Differences between (a) standard convolution (Conv) and depthwise separable convolution (DSConv), which consists of (b) depthwise convolution and (c) pointwise convolution.

D. Volume Self-Training

Random forest, effective even with small training datasets [45], is employed to predict the volumetric quality based on the slice quality ratings. Both labeled and unlabeled volumes are utilized to train the random forest. The initial quality ratings of unlabeled volumes are determined based on the following rules: 1) “Pass” if more than 80 percent of the slices in the volume are labeled as “pass”; 2) “Fail” if more slices are labeled as “fail” than “pass” or “questionable”; 3) “Questionable” if otherwise.

Similar to slice self-training, volume self-training involves iterative volume relabeling/pruning, random forest retraining (blue box in Fig. 1). The input to the random forest is the slice quality ratings predicted using the NR-Net. To reduce the influence of label noise, volumes satisfying the following criteria are retained: 1) Predicted labels identical to those predicted in the previous iteration; 2) Predicted labels with high-confidence, i.e., maximal probabilities beyond a threshold. The labels of the selected volumes are replaced by the predicted labels. Volumes that do not meet these criteria are pruned from the training dataset. The random forest is then retrained for the next iteration until accuracy improvement is minimal.

IV. EXPERIMENTAL RESULTS

A. Training

We evaluated our automatic IQA framework on T1- and T2-weighted MR images of pediatric subjects from birth to six years of age [46]. The images were separated into three datasets: 1) Training dataset with noisy labels (annotated volume-wise by an expert); 2) Testing dataset with reliable labels (annotated volume-wise by multiple experts); and 3) Unlabeled dataset. See Table I for a summary. Note that, as in practical scenarios, the unlabeled dataset is much larger. Fig. 4 shows examples of slices labeled as “pass” (no/minor artifacts), “questionable” (moderate artifacts), and “fail” (heavy artifacts).

In total, 3600, 2400, and 26040 axial slices were extracted, respectively, from the 60 T1-weighted training volumes, 40 T1-weighted testing volumes, and 434 T1-weighted unlabeled volumes. On the other hand, 3600, 2400, and 22800 axial slices were extracted, respectively, from the 60 T2-weighted

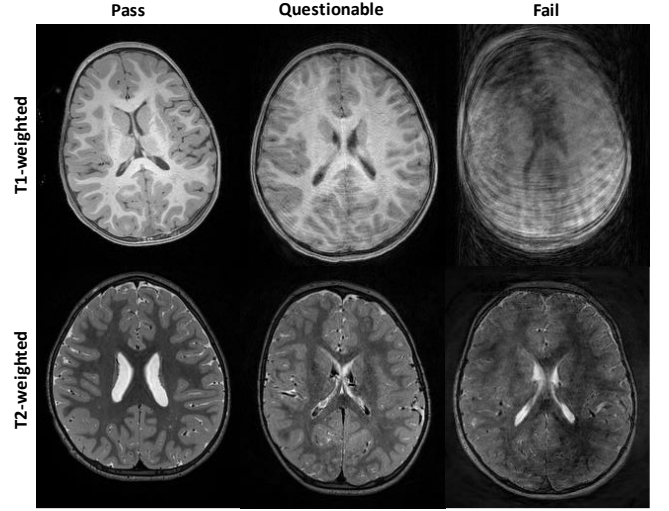


Fig. 4. Examples of T1- and T2-weighted slices labeled as “pass” (no/minor artifacts), “questionable” (moderate artifacts), and “fail” (heavy artifacts).

TABLE I
DATASETS FOR TRAINING AND TESTING

Data Type	Labeled Dataset						Unlabeled Dataset	
	Training Dataset			Testing Dataset				
	Pass	Ques	Fail	Pass	Ques	Fail		
T1w	20	20	20	25	9	6	434	
T2w	20	20	20	21	6	13	380	

training volumes, 40 T2-weighted testing volume, and 380 T2-weighted unlabeled volumes. Each slice was uniformly padded to 256×256 , min-max intensity normalized, and labeled according to the volume it belongs to. For both slice and volume assessments, the T1-/T2-weighted slice/volume training sets were divided into training and validation subsets with a ratio of 9:1.

To implement NR-Net, we employed Keras with Tensorflow backend. To avoid overfitting, the data were augmented via rotation and horizontal flipping. In addition, L_2 regularization was used for the Conv and DSConv layers. To deal with data imbalance, a multi-class balanced focal loss [47] with

TABLE II
COMPARISON OF DIFFERENT THRESHOLDS

(a) Threshold Comparison for T1-Weighted Images

p_{slice}	p_{volume}			
	0.6	0.7	0.8	0.9
0.6	0.8750	0.9000	0.9000	0.8750
0.7	0.9750	1.0000	1.0000	1.0000
0.8	0.9750	1.0000	1.0000	1.0000
0.9	0.9750	1.0000	1.0000	1.0000

(b) Threshold Comparison for T2-Weighted Images

p_{slice}	p_{volume}			
	0.6	0.7	0.8	0.9
0.6	0.8250	0.8250	0.8750	0.8750
0.7	0.9250	1.0000	1.0000	1.0000
0.8	0.9250	1.0000	1.0000	1.0000
0.9	0.9250	1.0000	1.0000	1.0000

L_2 regularization was used:

$$\mathcal{L}(p_t) = -\alpha_t(1-p_t)^\kappa \log(p_t) + \frac{\lambda}{2n_w} \sum_w \|w\|_2^2, \quad (3)$$

where p_t , $t = 1, 2, 3$, are the predicted probabilities for “pass”, “questionable”, and “fail”. $\kappa \geq 0$ is a focusing parameter, w 's are the weight matrices of NR-Net, $\lambda = 0.01$ is a tuning parameter for L_2 regularization, and n_w is the number of weight matrices. Here, the class weights $\alpha_t = \max(N_1, N_2, N_3)/N_t$ are used for balancing the contributions of imbalanced datasets. N_t is the number of slices in association with the t -th class. The RMSprop optimizer was employed to learn the network weights, with the initial learning rate set to 1×10^{-5} and the decay rate set to 5×10^{-8} . Slice self-training was repeated twice.

Random forest for volume prediction was implemented using Scikit-Learn. The random forest consisted of 50 trees with entropy as a measure of quality. Balanced class weights were used to counter volume data imbalance. Volume self-training was repeated twice.

B. Determination of Thresholds

Utilizing semi-supervised learning (Section IV-A), we obtained 29640 and 26400 T1-weighted and T2-weighted slices labeled with “pass”, “questionable” or “fail”. These slices were then used for slice and volume self-training, considering 4 probability thresholds $p_{\text{slice}}, p_{\text{volume}} \in \{0.6, 0.7, 0.8, 0.9\}$. Table II shows that the prediction accuracy is stable when the threshold is 0.7 and greater. Thus, in subsequent experiments, we set both p_{slice} and p_{volume} to 0.8.

C. Ablation Study

To verify the effectiveness of DSRes and NRes blocks, we compared modified versions of NR-Net:

- Convolution residual (CRes) network, which substitutes the DSRes blocks and NRes block with CRes blocks with channel numbers 128, 256 and 512;

TABLE III
NUMBER OF PARAMETERS (NoP), MAXIMAL DIMENSION (MD), AND TIME COST (TC) ON GPU AND CPU.

Network	NoP	MD	TC (Slice)		TC (Volume)	
			GPU	CPU	GPU	CPU
CRes	4.86M	512	10.71ms	0.228s	355ms	11.635s
CRes+NRes	1.31M	256	10.35ms	0.197s	333ms	10.251s
DSRes	0.75M	512	10.58ms	0.175s	347ms	7.874s
DSRes+NRes	0.33M	256	10.01ms	0.159s	312ms	6.723s

- CRes+NRes network, which substitutes DSRes blocks with CRes blocks with channel numbers 128 and 256;
- DSRes network, which substitutes the NRes block with DSRes block with channel number 512.

Note that NR-Net is a DSRes+NRes network. These networks were trained in a manner similar to the NR-Net.

1) *Computational Efficiency*: We compared the computational efficiency of NR-Net (DSRes+NRes network) with the other networks using several metrics: Number of parameters (NoP), the maximal dimension (MD), GPU and CPU time costs (TCs) of slice and volume. An NVIDIA GeForce GTX 1080Ti (GPU) and an Intel i7-8700K (CPU) were used for evaluation.

As shown in Table III, the NoP and TCs of NR-Net (DSRes+NRes network) are much smaller than the other networks (e.g., 14× times smaller than CRes) and the CPU TC of each slice and volume is ∼1.5 times lower. Compared with CRes and CRes+NRes, the NRes block reduces the maximal dimension from 512 to 256 and reduces the NoP by over three times. The GPU and CPU TCs of slice and volume are reduced by over 3%, and particularly both the CPU slice and volume TC are reduced by over 11.8%. Compared with the NoP and TCs of DSRes, the NoP of DSRes+NRes is reduced by over 2 times. The GPU and CPU TCs of slice and volume are all reduced by over 5%, particularly the CPU volume TC, which is reduced by over 15%. CRes and DSRes have the same maximal dimension. The NoP of DSRes is over 6 times smaller than CRes. Comparing the TCs of CRes and DSRes, the reduction of TCs on GPU is only ∼2%, but on CPU it is quite significant, i.e., ∼23% and ∼33% reduction of slice and volume TCs, respectively. Similarly, comparing CRes+NRes and DSRes+NRes, the NoP reduction reaches almost 4 times and the reduction of GPU and CPU TCs reaches over 3% and 20%, respectively. The analysis above shows that DSRes block and NRes block improve the computational efficiency of the overall network, making it suitable for real-time IQA.

2) *Network Efficiency*: Tables IV and V show the confusion matrices, along with the sensitivity and specificity of the different methods for T1-weighted testing images. The corresponding results for T2-weighted testing images are shown in Tables VI and VII. The detailed IQA results for the testing T1- and T2-weighted images are shown in Figs. 5 and 6, respectively.

It can be observed from Tables IV and V that the proposed method yields the best volume IQA performance than the other methods in terms of sensitivity and specificity. The slice

TABLE IV
CONFUSION MATRICES OF CRES, CRES+NRES, DSRES AND DSRES+NRES FOR T1-WEIGHTED IMAGES

Image Quality		Predicted					
		Pass		Ques		Fail	
		Slice	Volume	Slice	Volume	Slice	Volume
Actual	Pass	1421	23	79	2	0	0
	Ques	-	0	-	9	-	0
	Fail	0	0	3	0	357	6
Image Quality		Predicted					
		Pass		Ques		Fail	
		Slice	Volume	Slice	Volume	Slice	Volume
Actual	Pass	1470	24	30	1	0	0
	Ques	-	0	-	9	-	0
	Fail	0	0	6	0	354	6

Image Quality		Predicted					
		Pass		Ques		Fail	
		Slice	Volume	Slice	Volume	Slice	Volume
Actual	Pass	1437	24	62	1	1	0
	Ques	-	0	-	9	-	0
	Fail	0	0	5	0	355	6

Image Quality		Predicted					
		Pass		Ques		Fail	
		Slice	Volume	Slice	Volume	Slice	Volume
Actual	Pass	1500	25	0	0	0	0
	Ques	-	0	-	9	-	0
	Fail	0	0	56	0	304	6

TABLE V
SENSITIVITY AND SPECIFICITY OF CRES, CRES+NRES, DSRES AND DSRES+NRES FOR T1-WEIGHTED IMAGES

Image Quality		Sensitivity		Specificity	
		Slice	Volume	Slice	Volume
		Pass	Ques	Fail	Pass
Image Quality	Pass	0.9473	0.9200	1.0000	1.0000
	Ques	-	1.0000	-	0.9355
	Fail	0.9917	1.0000	1.0000	1.0000
Image Quality		Sensitivity		Specificity	
		Slice	Volume	Slice	Volume
		Pass	Ques	Fail	Pass
Image Quality	Pass	0.9800	0.9600	1.0000	1.0000
	Ques	-	1.0000	-	0.9667
	Fail	0.9833	1.0000	1.0000	1.0000

Image Quality		Sensitivity		Specificity	
		Slice	Volume	Slice	Volume
		Pass	Ques	Fail	Pass
Image Quality	Pass	0.9580	0.9600	1.0000	1.0000
	Ques	-	1.0000	-	0.9677
	Fail	0.9861	1.0000	0.9993	1.0000

Image Quality		Sensitivity		Specificity	
		Slice	Volume	Slice	Volume
		Pass	Ques	Fail	Pass
Image Quality	Pass	1.0000	1.0000	1.0000	1.0000
	Ques	-	1.0000	-	1.0000
	Fail	0.8444	1.0000	1.0000	1.0000

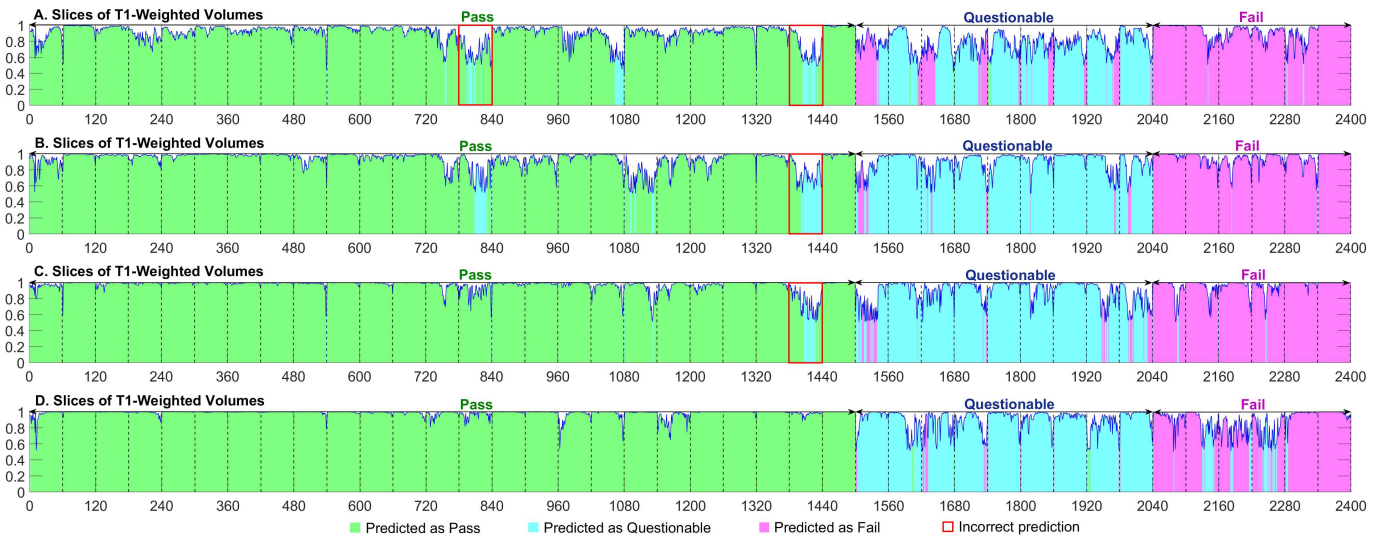


Fig. 5. Quality assessment of T1-weighted images. (A) CRes, (B) CRes+NRes, (C) DSRes, and (D) DSRes+NRes. The slices of each volume are marked by dashed vertical lines.

prediction results in Tables IV and V and Fig. 5 show that the sensitivity of “fail” slices for DSRes+NRes method is

lower than the other methods. This however does not affect the sensitivity of volume IQA. Similar conclusions can be drawn

TABLE VI
CONFUSION MATRICES OF CRES, CRES+NRES, DSRES AND DSRES+NRES FOR T2-WEIGHTED IMAGES

Image Quality		Predicted					
		Pass		Ques		Fail	
		Slice	Volume	Slice	Volume	Slice	Volume
Actual	Pass	1243	21	12	0	5	0
	Ques	-	1	-	4	-	1
	Fail	0	0	0	0	780	13

Image Quality		Predicted					
		Pass		Ques		Fail	
		Slice	Volume	Slice	Volume	Slice	Volume
Actual	Pass	1257	21	3	0	0	0
	Ques	-	2	-	4	-	0
	Fail	0	0	6	0	774	13

Image Quality		Predicted					
		Pass		Ques		Fail	
		Slice	Volume	Slice	Volume	Slice	Volume
Actual	Pass	1242	21	15	0	3	0
	Ques	-	1	-	3	-	2
	Fail	0	0	6	0	774	13

Image Quality		Predicted					
		Pass		Ques		Fail	
		Slice	Volume	Slice	Volume	Slice	Volume
Actual	Pass	1248	21	12	0	0	0
	Ques	-	0	-	6	-	0
	Fail	0	0	0	0	780	13

TABLE VII
SENSITIVITY AND SPECIFICITY OF CRES, CRES+NRES, DSRES AND DSRES+NRES FOR T2-WEIGHTED IMAGES

Image Quality		Sensitivity		Specificity	
		Slice	Volume	Slice	Volume
		Pass	1.0000	1.0000	0.9474
Actual	Ques	-	0.6667	-	1.0000
	Fail	1.0000	1.0000	0.9960	0.9630

Image Quality		Sensitivity		Specificity	
		Slice	Volume	Slice	Volume
		Pass	1.0000	1.0000	0.8947
Actual	Ques	-	0.6667	-	1.0000
	Fail	0.9923	1.0000	1.0000	1.0000

Image Quality		Sensitivity		Specificity	
		Slice	Volume	Slice	Volume
		Pass	1.0000	1.0000	0.9474
Actual	Ques	-	0.5000	-	1.0000
	Fail	0.9923	1.0000	0.9976	0.9259

Image Quality		Sensitivity		Specificity	
		Slice	Volume	Slice	Volume
		Pass	1.0000	1.0000	1.0000
Actual	Ques	-	1.0000	-	1.0000
	Fail	1.0000	1.0000	1.0000	1.0000

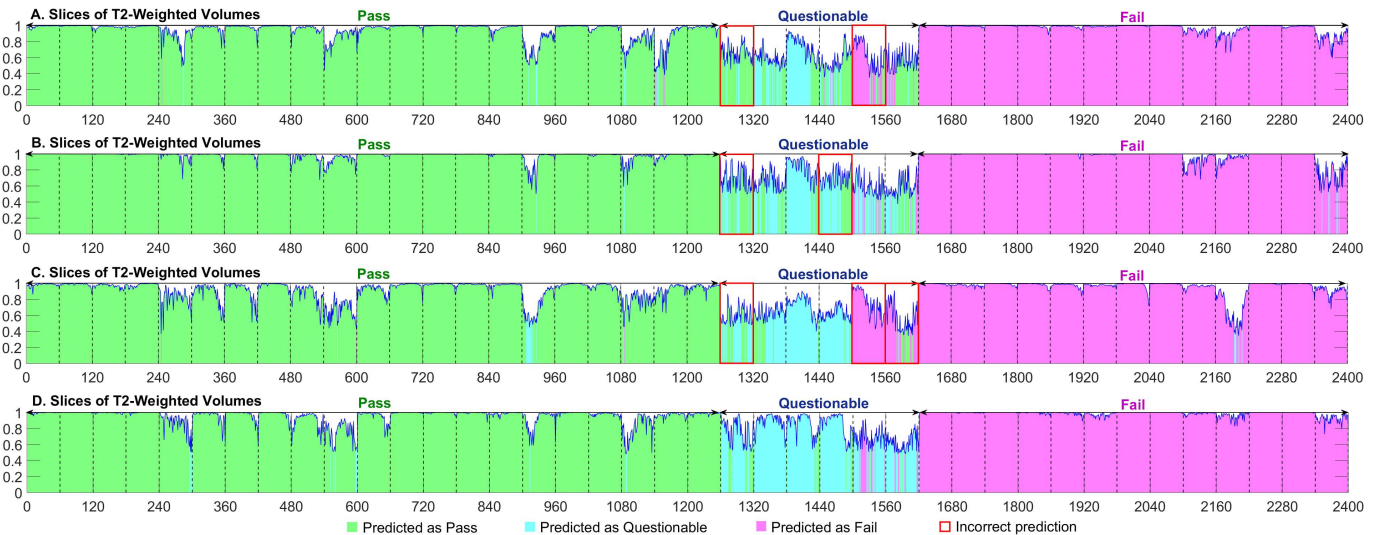


Fig. 6. Quality assessment of T2-weighted images. (A) CRes, (B) CRes+NRes, (C) DSRes, and (D) DSRes+NRes. The slices of each volume are marked by dashed vertical lines.

for T2-weighted images from Tables VI and VII and Fig. 6, showing that the proposed method consistently yields the best

performance for volume IQA.

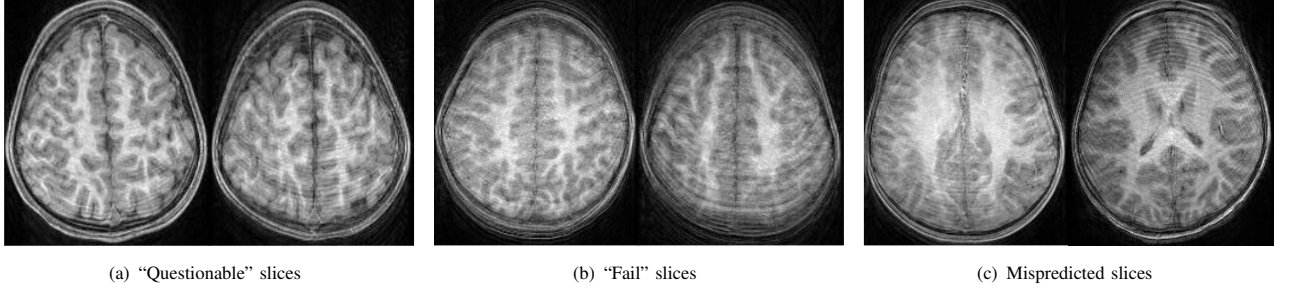


Fig. 7. Examples of “questionable”, “fail”, and mispredicted T1-weighted slices.

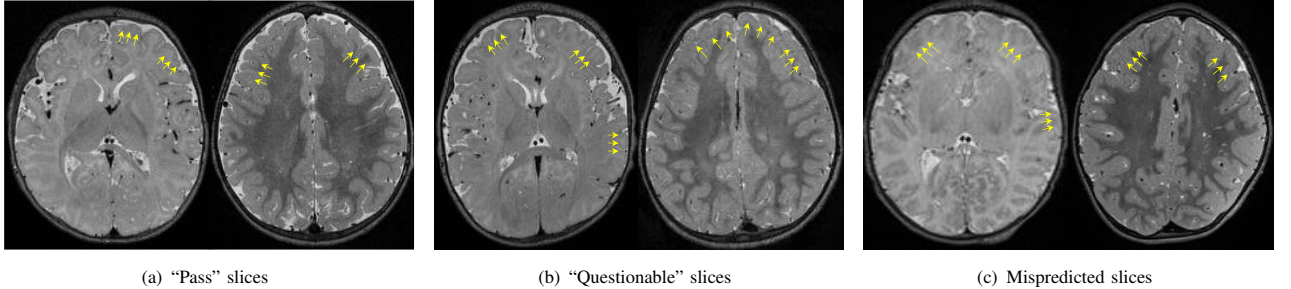


Fig. 8. Examples of “pass”, “questionable”, and mispredicted T2-weighted slices. The arrows mark some artifacts.

D. Discordant Case Analysis

It can be observed from Table IV(d) and Fig. 5-D that “fail” T1-weighted slices can be mistakenly predicted as “questionable”. By retrospectively inspecting all “questionable” and “fail” T1-weighted training slices, we found that this confusion is caused by the existence of ringing and motion artifacts in most “questionable” and “fail” slices, as shown in Fig. 7. Similarly, it can be observed from Table VI(d) and Fig. 6-D that “pass” T2-weighted slices can sometimes be mispredicted as “questionable”. Subtle degradation such as contrast reduction and local fuzziness can confuse the IQA network and causes mispredictions as shown in Fig. 8.

E. Performance Comparison

To verify the effectiveness of the proposed IQA method, we compared it with several deep learning IQA methods:

- Pretrained and fine-tuned [31]: InceptionV4 [48], ResNet [49]
- Trained from scratch: CNN [29]

For volume-wise IQA, our random forest is applied to the slice-wise quality ratings given by these methods.

Figs. 9 and 10, respectively, shows the evaluation results in terms of sensitivity (SEN), specificity (SPE), and accuracy (ACC) for slice- and volume-wise IQA of the T1- and T2-weighted testing data. From Figs. 9 and 10, our method significantly outperforms all compared methods for all evaluation metrics except sensitivity to “fail” T1-weighted slices (i.e., SEN-S-F).

F. Effectiveness of Semi-Supervised Learning

We evaluated whether semi-supervised learning is able to correctly assess of the large amount of unlabeled data. The

TABLE VIII
EFFECTIVENESS OF SEMI-SUPERVISED LEARNING

Image Quality		Predicted			Sensitivity	Specificity
		Pass	Ques	Fail		
Label	Pass	319	1	0	0.9969	0.9561
	Ques	5	79	0	0.9405	0.9971
	Fail	0	0	30	1.0000	1.0000

Image Quality		Predicted			Sensitivity	Specificity
		Pass	Ques	Fail		
Label	Pass	169	5	0	0.9713	0.9903
	Ques	2	145	0	0.9864	0.9831
	Fail	0	0	59	1.0000	1.0000

unlabeled data were annotated by an expert and the labels were compared with the predictions given by our method. As can be observed from Table VIII, the automated and predicted volume IQA results are largely consistent. This implies that our method is able to effectively harness the large amount of unlabeled data for increasing sample size and hence improving network training.

V. DISCUSSION AND CONCLUSION

In this paper, we have proposed a deep learning method for IQA of pediatric T1- and T2-weighted MR images. The network consists of a nonlocal residual network (NR-Net) for slice IQA and a random forest for volume IQA. Our method requires only a small amount of quality-annotated images for pre-training the NR-Net for initial automated annotation of a large amount of unlabeled dataset. This is refined via

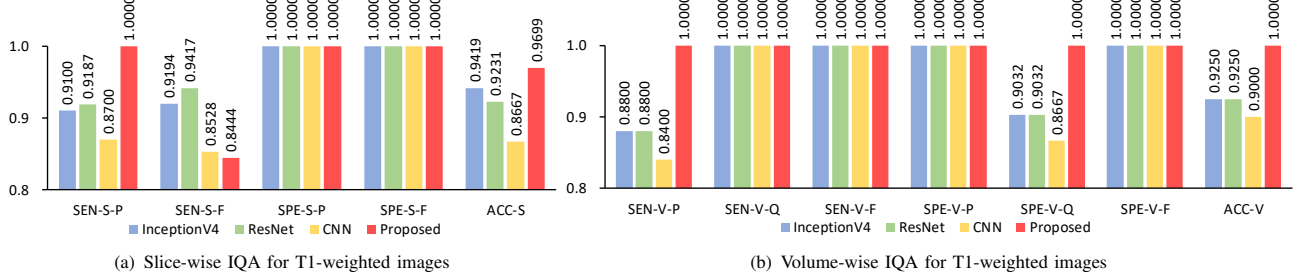


Fig. 9. Slice- and volume-wise IQA for T1-weighted images. Evaluation metrics are denoted in the following form: metric (SEN/SPE/ACC) - stage (S/V) - quality (P/Q/F/-).

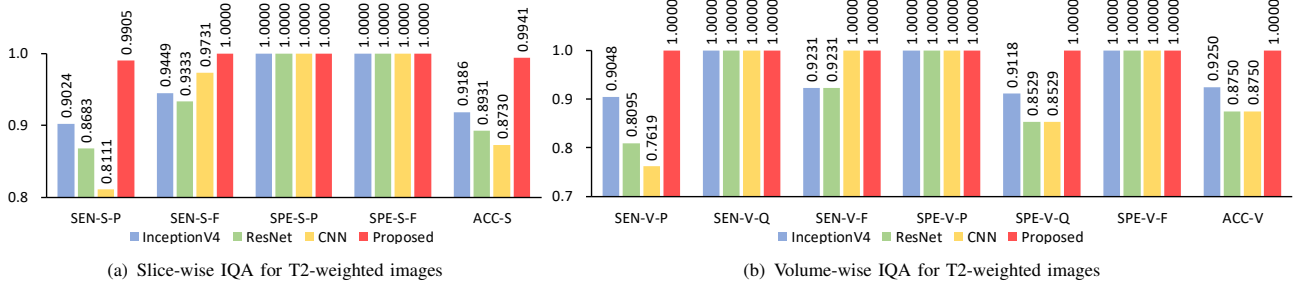


Fig. 10. Slice- and volume-wise IQA for T2-weighted images. Evaluation metrics are denoted in the following form: metric (SEN/SPE/ACC) - stage (S/V) - quality (P/Q/F/-).

subsequent self-training processes. Our method copes with label noise effectively, affords tolerance to inevitable rater errors, minimizes the amount of required label data, and reduces the number of manual labeling hours. Experimental results verify that the proposed method yields near perfect IQA accuracy at a very low computational cost.

The proposed two-stage method is flexible and can be adjusted according to data availability. When only slice labels are available, NR-Net can be trained for slice IQA. When only volume labels are available, the two-stage framework can be used to identify slices that are useful for network training for slice and volume IQA. When a large labeled dataset is available, the semi-supervised learning process can be omitted. When a small labeled dataset and a large unlabeled dataset are available, the whole proposed framework can be utilized.

The proposed method can be combined with quality enhancement methods, such as artifact removal methods, for integrated quality control. The proposed framework can also be adapted to other IQA tasks, for instance, the IQA of diffusion MRI, where the size of unlabeled data is typically larger than that of labeled data, and where label noise is a significant issue. Future efforts will be directed towards such extension of our method.

ACKNOWLEDGEMENT

This work was supported in part by NIH grants (AG053867, EB006733, MH117943, MH104324, and MH110274) and the efforts of the UNC/UMN Baby Connectome Project Consortium.

REFERENCES

- [1] J. Zhuo and R. P. Gullapalli, "MR artifacts, safety, and quality control," *RadioGraphics*, vol. 26, no. 1, pp. 275–297, Jan. 2006.
- [2] Q. Huynh-Thu, M.-N. Garcia, F. Speranza, P. Corriveau, and A. Raake, "Study of rating scales for subjective quality assessment of high-definition video," *IEEE Transactions on Broadcasting*, vol. 57, no. 1, pp. 1–14, mar 2011.
- [3] T. Kustner, P. Wolf, M. Schwartz, A. Liebgott, F. Schick, S. Gatidis, and B. Yang, "An easy-to-use image labeling platform for automatic magnetic resonance image quality assessment," in *Proceedings of IEEE 14th International Symposium on Biomedical Imaging (ISBI)*. IEEE, Apr. 2017.
- [4] T. White, P. R. Jansen, R. L. Muetzel, G. Sudre, H. E. Marroun, H. Tiemeier, A. Qiu, P. Shaw, A. M. Michael, and F. C. Verhulst, "Automated quality assessment of structural magnetic resonance images in children: Comparison with visual inspection and surface-based reconstruction," *Human Brain Mapping*, vol. 39, no. 3, pp. 1218–1231, dec 2017.
- [5] E. L. Gedamu, D. Collins, and D. L. Arnold, "Automated quality control of brain MR images," *Journal of Magnetic Resonance Imaging*, vol. 28, no. 2, pp. 308–319, Aug. 2008.
- [6] Z. W. Abdul Rehman, "Reduced-reference image quality assessment by structural similarity estimation," *IEEE Transactions on Image Processing*, vol. 21, no. 8, pp. 3378–3389, May 2012.
- [7] R. A. Manap and L. Shao, "Non-distortion-specific no-reference image quality assessment: A survey," *Information Sciences*, vol. 301, pp. 141–160, Apr. 2015.
- [8] P. Ye and D. Doermann, "No-reference image quality assessment using visual codebooks," *IEEE Transactions on Image Processing*, vol. 21, no. 7, pp. 3129–3138, Jul. 2012.
- [9] H. Tang, N. Joshi, and A. Kapoor, "Learning a blind measure of perceptual image quality," in *Proceedings of IEEE Conference on Computer Vision and Pattern Recognition (CVPR)*, Colorado Springs, USA, Jun. 2011, pp. 305–312.
- [10] M. A. Saad, A. C. Bovik, and C. Charrier, "Blind image quality assessment: A natural scene statistics approach in the DCT domain," *IEEE Transactions on Image Processing*, vol. 21, no. 8, pp. 3339–3352, Aug. 2012.
- [11] J. Kim, H. Zeng, D. Ghadiyaram, S. Lee, L. Zhang, and A. C. Bovik, "Deep convolutional neural models for picture-quality prediction: Challenges and solutions to data-driven image quality assessment," *IEEE Signal Processing Magazine*, vol. 34, no. 6, pp. 130–141, Nov. 2017.
- [12] F. Chollet, "Xception: Deep learning with depthwise separable convolutions," in *Proceedings of IEEE Conference on Computer Vision and Pattern Recognition (CVPR)*, Honolulu, USA, Jul. 2017, pp. 1800–1807.
- [13] X. Wang, R. Girshick, A. Gupta, and K. He, "Non-local neural net-

- works,” in *Proceedings of IEEE Conference on Computer Vision and Pattern Recognition (CVPR)*, Salt Lake City, USA, Jun. 2018, pp. 7794–7803.
- [14] X. Yang, F. Li, and H. Liu, “A survey of DNN methods for blind image quality assessment,” *IEEE Access*, vol. 7, pp. 123 788–123 806, 2019.
- [15] X. Liu, J. V. D. Weijer, and A. D. Bagdanov, “RankIQA: Learning from rankings for no-reference image quality assessment,” in *Proceedings of IEEE International Conference on Computer Vision (ICCV)*. IEEE, oct 2017.
- [16] K.-Y. Lin and G. Wang, “Hallucinated-IQA: No-reference image quality assessment via adversarial learning,” in *Proceedings of IEEE Conference on Computer Vision and Pattern Recognition (CVPR)*, Jun. 2018.
- [17] K. Ma, W. Liu, K. Zhang, Z. Duanmu, Z. Wang, and W. Zuo, “End-to-end blind image quality assessment using deep neural networks,” *IEEE Transactions on Image Processing*, vol. 27, no. 3, pp. 1202–1213, Mar. 2018.
- [18] J. Kim, A.-D. Nguyen, S. Ahn, C. Luo, and S. Lee, “Multiple level feature-based universal blind image quality assessment model,” in *Proceedings of IEEE International Conference on Image Processing (ICIP)*, Oct. 2018.
- [19] W. Zhang, K. Ma, J. Yan, D. Deng, and Z. Wang, “Blind image quality assessment using a deep bilinear convolutional neural network,” *IEEE Transactions on Circuits and Systems for Video Technology*, vol. 30, no. 1, pp. 36–47, jan 2020.
- [20] J. Guan, S. Yi, X. Zeng, W.-K. Cham, and X. Wang, “Visual importance and distortion guided deep image quality assessment framework,” *IEEE Transactions on Multimedia*, vol. 19, no. 11, pp. 2505–2520, Nov. 2017.
- [21] S. Bosse, D. Maniry, K.-R. Muller, T. Wiegand, and W. Samek, “Deep neural networks for no-reference and full-reference image quality assessment,” *IEEE Transactions on Image Processing*, vol. 27, no. 1, pp. 206–219, jan 2018.
- [22] Q. Yan, D. Gong, and Y. Zhang, “Two-stream convolutional networks for blind image quality assessment,” *IEEE Transactions on Image Processing*, vol. 28, no. 5, pp. 2200–2211, may 2019.
- [23] J. Kim, A.-D. Nguyen, and S. Lee, “Deep CNN-based blind image quality predictor,” *IEEE Transactions on Neural Networks and Learning Systems*, vol. 30, no. 1, pp. 11–24, Jan. 2019.
- [24] W. Hou, X. Gao, D. Tao, and X. Li, “Blind image quality assessment via deep learning,” *IEEE Transactions on Neural Networks and Learning Systems*, vol. 26, no. 6, pp. 1275–1286, jun 2015.
- [25] W. Hou and X. Gao, “Saliency-guided deep framework for image quality assessment,” *IEEE MultiMedia*, vol. 22, no. 2, pp. 46–55, apr 2015.
- [26] Y. Li, L.-M. Po, X. Xu, L. Feng, F. Yuan, C.-H. Cheung, and K.-W. Cheung, “No-reference image quality assessment with shearlet transform and deep neural networks,” *Neurocomputing*, vol. 154, pp. 94–109, apr 2015.
- [27] R. A. Pizarro, X. Cheng, A. Barnett, H. Lemaitre, B. A. Verchinski, A. L. Goldman, E. Xiao, Q. Luo, K. F. Berman, J. H. Callicott, D. R. Weinberger, and V. S. Mattay, “Automated quality assessment of structural magnetic resonance brain images based on a supervised machine learning algorithm,” *Frontiers in Neuroinformatics*, vol. 10, Dec. 2016.
- [28] S. Bianco, L. Celona, P. Napoletano, and R. Schettini, “On the use of deep learning for blind image quality assessment,” *Signal, Image and Video Processing*, vol. 12, no. 2, pp. 355–362, Aug. 2017.
- [29] S. J. Esses, X. Lu, T. Zhao, K. Shanbhogue, B. Dane, M. Bruno, and H. Chandarana, “Automated image quality evaluation of T2-weighted liver MRI utilizing deep learning architecture,” *Journal of Magnetic Resonance Imaging*, vol. 47, no. 3, pp. 723–728, jun 2017.
- [30] J. Gu, G. Meng, J. A. Redi, S. Xiang, and C. Pan, “Blind image quality assessment via vector regression and object oriented pooling,” *IEEE Transactions on Multimedia*, vol. 20, no. 5, pp. 1140–1153, may 2018.
- [31] P. B. S. M. Muellly and S. S. Vasanwala, “Automated quality control of mr images using deep convolutional neural networks,” in *Proceedings of International Society for Magnetic Resonance in Medicine (ISMRM)*, Honolulu, USA, Apr. 2017, pp. 1–3.
- [32] T. Kstner, A. Liebgott, L. Mauch, P. Martirosian, F. Bamberg, K. Nikolaou, B. Yang, F. Schick, and S. Gatidis, “Automated reference-free detection of motion artifacts in magnetic resonance images,” *Magnetic Resonance Materials in Physics, Biology and Medicine*, vol. 31, no. 2, pp. 243–256, Sep. 2017.
- [33] Y. Ding, S. Suffren, P. Bellec, and G. A. Lodygensky, “Supervised machine learning quality control for magnetic resonance artifacts in neonatal data sets,” *Human Brain Mapping*, vol. 40, no. 4, pp. 1290–1297, nov 2018.
- [34] B. Frenay and M. Verleysen, “Classification in the presence of label noise: A survey,” *IEEE Transactions on Neural Networks and Learning Systems*, vol. 25, no. 5, pp. 845–869, May 2014.
- [35] S. Reed, H. Lee, D. Anguelov, C. Szegedy, D. Erhan, and A. Rabinovich, “Training deep neural networks on noisy labels with bootstrapping,” *CoRR*, vol. abs/1412.6596, 2014.
- [36] Y. Li, J. Yang, Y. Song, L. Cao, J. Luo, and L.-J. Li, “Learning from noisy labels with distillation,” in *Proceedings of IEEE International Conference on Computer Vision (ICCV)*, Venice, Italy, Oct. 2017, pp. 1910–1918.
- [37] G. Patrini, A. Rozza, A. K. Menon, R. Nock, and L. Qu, “Making deep neural networks robust to label noise: A loss correction approach,” in *Proceedings of IEEE Conference on Computer Vision and Pattern Recognition (CVPR)*, Honolulu, USA, Jul. 2017, pp. 1944–1952.
- [38] S. Cuendet, D. Hakkani-Tr, and E. Shriberg, “Automatic labeling inconsistencies detection and correction for sentence unit segmentation in conversational speech,” in *Proceedings of MLMI on Machine Learning for Multimodal Interaction*, Brno, Czech Republic, Jun. 2007, pp. 144–155.
- [39] A. L. B. Miranda, L. P. F. Garcia, A. C. P. L. F. Carvalho, and A. C. Lorena, “Use of classification algorithms in noise detection and elimination,” in *Proceedings of International Conference on Hybrid Artificial Intelligence Systems*, Salamanca, Spain, 2009, pp. 417–424.
- [40] C. Seiffert, T. M. Khoshgoftaar, J. V. Hulse, and A. Folleco, “An empirical study of the classification performance of learners on imbalanced and noisy software quality data,” *Information Sciences*, vol. 259, pp. 571–595, Feb. 2014.
- [41] F. O. Kaster, B. H. Menze, M.-A. Weber, and F. A. Hamprecht, “Comparative validation of graphical models for learning tumor segmentations from noisy manual annotations,” in *Proceedings of International MICCAI Workshop on Medical Computer Vision*, Athens, Greece, Oct. 2011, pp. 74–85.
- [42] R. Xu and D. WunschII, “Survey of clustering algorithms,” *IEEE Transactions on Neural Networks*, vol. 16, no. 3, pp. 645–678, May 2005.
- [43] V. Mnih and G. E. Hinton, “Learning to label aerial images from noisy data,” in *Proceedings of International Conference on Machine Learning (ICML)*, Edinburgh, Scotland, Jun. 2012, pp. 203–210.
- [44] Q. Miao, Y. Cao, G. Xia, M. Gong, J. Liu, and J. Song, “RBoost: Label noise-robust boosting algorithm based on a nonconvex loss function and the numerically stable base learners,” *IEEE Transactions on Neural Networks and Learning Systems*, vol. 27, no. 11, pp. 2216–2228, Nov. 2016.
- [45] L. Breiman, “Random forest,” *Machine Learning*, vol. 45, no. 1, pp. 5–32, Oct. 2001.
- [46] B. R. Howell, M. A. Styner, W. Gao, P.-T. Yap, L. Wang, K. Baluyot, E. Yacoub, G. Chen, T. Potts, A. Salzwedel, G. Li, J. H. Gilmore, J. Piven, J. K. Smith, D. Shen, K. Ugurbil, H. Zhu, W. Lin, and J. T. Ellison, “The UNC/UMN baby connectome project (BCP): An overview of the study design and protocol development,” *NeuroImage*, vol. 185, pp. 891–905, Jan. 2019.
- [47] T.-Y. Lin, P. Goyal, R. Girshick, K. He, and P. Dollar, “Focal loss for dense object detection,” in *Proceedings of IEEE International Conference on Computer Vision (ICCV)*, Venice, Italy, Oct. 2017, pp. 2980–2988.
- [48] S. I. Christian Szegedy, “Inception-v4, inception-resnet and the impact of residual connections on learning,” in *Proceedings of AAAI Conference on Artificial Intelligence*, Feb. 2017, pp. 4278–4284.
- [49] K. He, X. Zhang, S. Ren, and J. Sun, “Deep residual learning for image recognition,” in *Proceedings of IEEE Conference on Computer Vision and Pattern Recognition (CVPR)*, Jun. 2016.